JOURNAL OF MATERIALS SCIENCE **38** (2003) 4041 – 4046

Study of nickel passivation in a borate medium

M. BOINET, S. MAXIMOVITCH, F. DALARD
Laboratoire d'Electrochimie et de Physico-Chimie des Matériaux et des Interfaces, UMR CNRS-INPG 5631, E.N.S.E.E.G., Domaine Universitaire, BP 75, 38402 Saint Martin D'Heres
E-mail: francis.dalard@lepmi.inpg.fr

O. DE BOUVIER
Département Etudes des Matériaux, Electricité de France, Centre de recherche des Renardières, 77818 Moret sur Loing

The adsorption of borate ions at the nickel and/or nickel oxide-electrolyte electrochemical interface was studied at various concentrations and pH values in lithium and borate solutions. First, the passivation range of nickel was estimated using cyclic voltammetry. The nickel passive layer formation kinetics (transfer resistance, capacitance of passive film formed, adsorption capacitance), as well as the semiconducting properties of this oxide layer, were studied using electrochemical impedance spectroscopy (E.I.S.). These electrochemical techniques were used in conjunction with adsorption measurements performed with an electrochemical quartz crystal microbalance (E.Q.C.M.) and with surface analyses (Auger spectroscopy). The nickel oxide showed type *p* semiconducting properties and was depleted at, corrosion potential. Moreover, very little borate adsorption was observed during the different tests. This may have been the result of the negative surface charge, in the pH and potential conditions applied.

1. Introduction

Optimising productivity, reducing maintenance costs and prolonging the service life of reactors (PWR) together represent a major economic challenge for the nuclear industry. During their service life, PWR reactors are subject to ageing leading to an asymmetric energy flux. One possible explanation for this phenomenon is the presence of nickel oxide deposits on the fuel rods (zirconium-based cladding). The source of these deposits is the corrosion of the nickel-based alloy fuel cladding tubes in the primary circuit. The addition of orthoboric acid (H_3BO_3) and lithium hydroxide (LiOH, H_2O) in the pure deoxygenated water of the primary circuit, could promote the adsorption of borates on nickel oxide deposits.

The present study concerns the adsorption of borates at the nickel and/or nickel oxide-electrolyte electrochemical interface as a function of their concentration in the aqueous phase and the pH value. Cyclic voltammetry measurements were performed in order to determine the passivation range of the nickel. Formation kinetics as well as the semiconducting properties of the passive film formed on the nickel in borate solution were characterised by Electrochemical Impedance Spectroscopy (E.I.S.). These electrochemical methods were used in conjunction with adsorption measurements performed using an Electrochemical Quartz Crystal Microbalance (E.Q.C.M.) and with surface analyses (Auger spectroscopy).

2. Experimental set-up and methods

The electrochemical measurements were performed in three different solutions representative of the primary circuit [1] (Table I), at 25°C, in a three-electrode electrochemical cell. The solutions were prepared from orthoboric acid (H_3BO_3 99%) and lithium hydroxide (LiOH, H_2O 98%), supplied by Prolabo. The working electrode was a nickel cylinder (Ni 99%, Goodfellow), 5 mm in diameter, embedded in PTFE and fitted to the cap of a Radiometer EDI 101T rotating disk electrode ($v_{rot} = 1000$ rpm). The auxiliary electrode was platinum and a Hg-HgO electrode was used as the reference ($E_{ref} = +117$ mV/SHE). All the potentials are refered to this electrode.

The nickel surface was ground with silicon carbide papers to 1200 grit. In order to start with a non-oxidised, reproducible surface before each test, the pre-existing nickel oxide was reduced (30 s) by cathodic reduction (Table I), with a potential shift taking into account the pH difference of these solutions.

The cyclic voltammetry measurements were performed with an EGG 273A potentiostat controlled by M352 or M270 software.

The E.I.S. measurements were obtained with a frequency response analyser and an electrochemical interface (Autolab), controlled by the FRA software application. Spectra were plotted at constant potentials by decreasing potential from 100 mV in the three previously defined study solutions. After potentiostatic

TABLE I Study solution and pre-treatment

	LiOH $mol \cdot L^{-1}$	H_3BO_3 $mol \cdot L^{-1}$	pH	Pre-treatment V/Hg-HgO
Solution 1	1.6×10^{-2}	—	12	−1.6
Solution 2	1.6×10^{-2}	9.25×10^{-2}	8.5	−1.39
Solution 3	1.6×10^{-2}	46.25×10^{-2}	7.15	−1.31

polarisation of the electrode for one hour at each measurement potential, a sinusoidal signal of 30 mV amplitude was applied with a frequency from 10 kHz to 0.01 Hz.

Adsorption measurements were performed using a Maxtek-PM 710 E.Q.C.M. Based on the piezoelectric properties of the quartz crystal, the E.Q.C.M. detects mass variations in the electrode through the frequency variations of the quartz according to Sauerbrey's equation [2]

$$\Delta f = -2f_0^2 \times \frac{\Delta m}{\sqrt{\mu_q \rho_q}} \quad (1)$$

where Δf: frequency variation caused by deposit (in Hz), f_0: resonant frequency (5 MHz) of the crystal quartz, Δm: mass variation linked deposit (in $g \cdot cm^{-2}$), μ_q: shear modulus of quartz (2.947×10^{11} $g \cdot cm^{-1} \cdot s^{-2}$), and ρ_q: density of quartz (2.648 $g \cdot cm^{-3}$).

A quartz crystal frequency variation of 1 Hz is equivalent to a mass variation of 18 $ng \cdot cm^{-2}$. This highly sensitive technique is well suited to the study of adsorbed species. The working electrode (1.37 cm^2) was a piezoelectric quartz crystal wafer, with a 0.33 μm thick gold coating for the gold electrode. The nickel electrode was then covered with a 0.2 μm thick nickel coating by vacuum evaporation. The auxiliary and reference electrodes were identical to those used for the electrochemical measurements.

To ensure the same initial surface conditions prior to each test, the two types of electrode were rinsed in alcohol and deionized water and a protocol was established to remove the species present on their surfaces. This involved electrochemical reconstruction for the gold electrode [3] and cathodic reduction (−1.72 V/Hg-HgO) for 30 s) for the nickel electrode. Finally, to check that the surface was reproducible between each measurement, the frequency of the quartz crystal was measured in deionized water, with the frequency obtained being used as a reference.

The Auger analyses were performed on an Auger spectrometer (Riber). Etching was carried out at 2.5 keV, either in sweep mode ($v_{déc} = 240$ Å $\cdot mn^{-1}$), or fixed mode ($v_{déc} = 3600$ Å $\cdot mn^{-1}$).

3. Experimental results

3.1. Cyclic voltammetry

Fig. 1 shows the voltammogram obtained for a nickel electrode in the three solutions. In solution 1, at pH 12, oxidation of the nickel started −0.77 V/Hg-HgO according to the following reaction:

$$Ni + 2OH^- \rightarrow Ni(OH)_2 + 2e^- \quad (2)$$

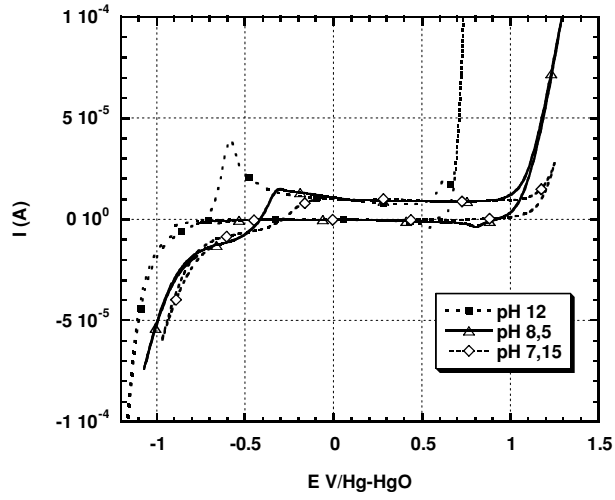

Figure 1 Cyclic voltammogram for nickel in solutions 1, 2 and 3 at 25°C ($v = 10$ mV/s).

The passivation range was between −0.42 V/Hg-HgO and 0.48 V/Hg-HgO. The current density values in this potential range were low, which might be related to the fact that oxide solubility is very low at pH = 12 [4]. In the transpassive region, the oxidation peak from nickel II to nickel III was observed at 0.63 V/Hg-HgO to the reaction:

$$Ni(OH)_2 \rightarrow NiOOH + H^+ + e^- \quad (3)$$

Reduction of the nickel III was observed at 0.53 V/Hg-HgO.

In solutions 2 and 3, the same characteristics with respect to the nickel oxidation reactions (reaction 2) were observed, with a potential shift attributed to the difference in pH. The passivation range was greater in these solutions (1 V at pH 8.5 and 1.1 V at pH 7.15). Nickel oxidation (reaction 3) was accompagnied by evolution of oxygen ($E > 1.08$ V/Hg-HgO) for both solutions. Reaction 3 in reduction ($E = 0.78$ V/Hg-HgO) was only visible in solution 2. These results are consistent with literature data [5].

3.2. Electrochemical impedance spectroscopy

Fig. 2 shows the characteristic Nyquist diagrams obtained at various potentials in solution 3. They are modelled by a one step electrosorption reaction [6] corresponding to the equivalent electric circuit in Fig. 3.

$$A^- + s \leftrightarrow A, s + e^- \quad (A^- : OH^-, \text{borates, etc.}) \quad (4)$$

Circuit parameters were determined using Z-VIEW software from Scribner Associates. To take into account dispersion phenomena, the capacitive terms are constant phase elements CPE. The observed Nyquist diagrams correspond to an adsorption capacitance (C_{ads}) of the same order of magnitude as an interfacial capacitance (C_{int}) The low frequency limit was not reached even for relatively low frequency values showing that the electrosorption reaction is slow. The electrolyte

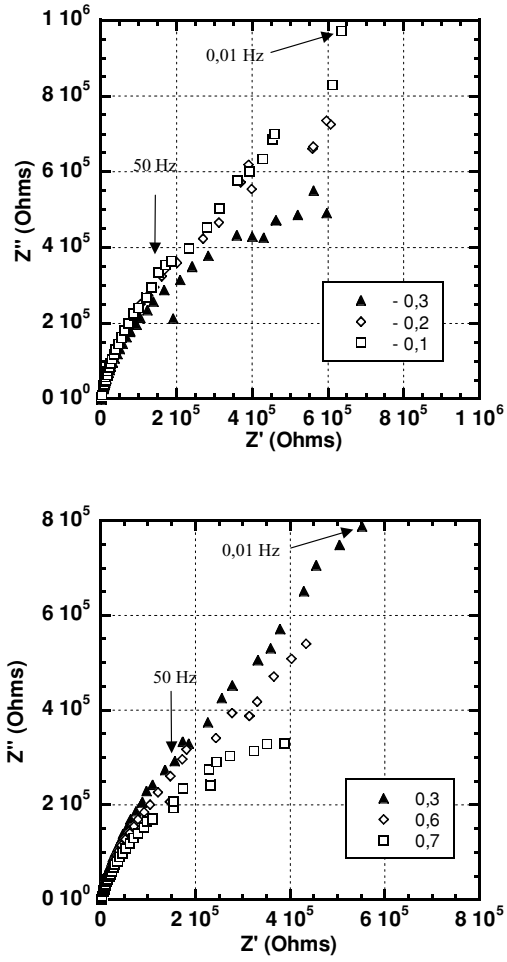

Figure 2 Nyquist diagrams in solution 3 (pH 7.15), at several potentials.

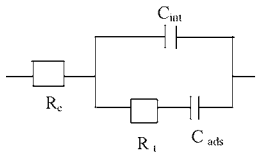

- R_t: transfer resistance,
- R_e: electrolyte resistance,
- C_{int}: interfacial capacitance,
- C_{ads}: adsorption capacitance.

Figure 3 Equivalent circuit.

resistance (R_e) and the interfacial capacitance (C_{int}) were determined from the high frequency part. The transfer resistance (R_t) and adsorption capacitance (C_{ads}) were then identified using the low frequency part.

R_e estimated in the three solutions (Table II), was found to increase when the pH was reduced. This variation reflects changes in the conductivity of the solutions, which increased when the borate ion concentration was higher. Thus, between pH 12 and pH 8.5, R_e increased because the conductivity of the solution decreased. In fact, at pH 12, the predominant species were $H_2BO_3^-$ ions, whereas at pH 8.5 and 7.15, the less concentrated $HB_4O_7^-$ ions were in a majority [7].

TABLE II Resistance of electrolyte in solutions 1, 2 and 3

	Solution 1 pH 12	Solution 2 pH 8.5	Solution 3 pH 7.15
Re (Ohms)	403	1677	1878

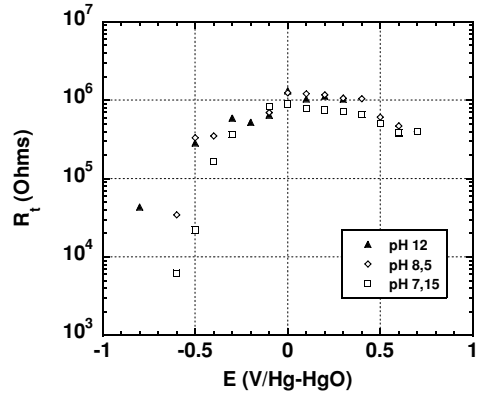

Figure 4 Changes in transfer resistance as a function of potential in the three solutions.

The changes in the transfer resistance (R_t) as a function of potential in the three solutions are shown in Fig. 4. The overall variation in transfer resistance was the same, irrespective of the pH. R_t was high and constant in the passive zone (10^6 ohms) where the conductivity in the film was the lowest [8]. The lower transfer resistance at potentials above 0.4 V/Hg-HgO is due to the properties of the nickel III oxide, which is more conductive than the nickel II oxide. In the water oxidation and reduction range, the transfer resistance dropped significantly, since the reactions involved are characterised by rapid kinetics. In this case, the equivalent circuit is no longer applicable.

Fig. 5 shows the changes in interfacial capacitance (C_{int}) as a function of potential. The variation was similar in all three solutions. In the absence of specific adsorption and surface states, the difference in potential at the passive film-electrolyte interface is distributed between the space charge region of the passive film and the Helmholtz layer [9]. The interface capacitance was thus equivalent to two capacitors in series: the capacitance of the space charge developed in the passive film (C_{SC}) and the Helmholtz layer capacitance (C_H):

$$1/C_{int} = 1/C_{SC} + 1/C_H \quad (5)$$

For potentials situated in the depleted region of majority carriers, the contribution of the Helmholtz layer

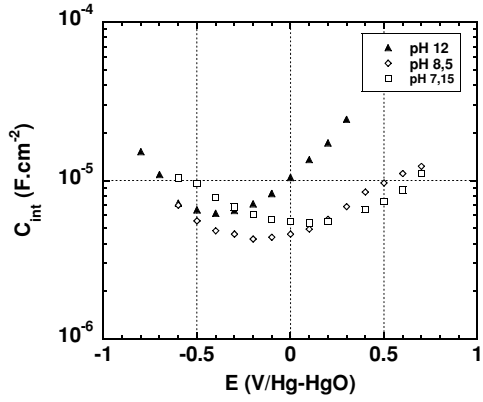

Figure 5 Changes in interfacial capacitance as a function of potential in the three solutions, for $f = 315.4$ Hz.

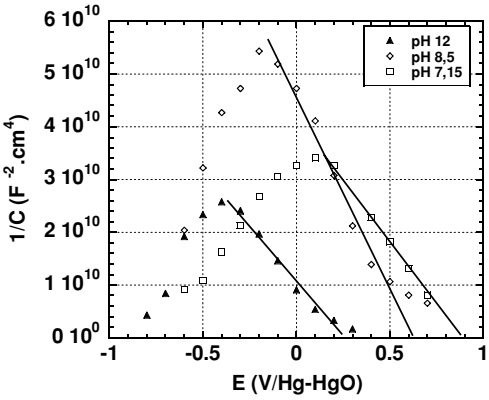

Figure 6 Mott-Schottky diagram in the three solutions, for $f =$ 315.4 Hz.

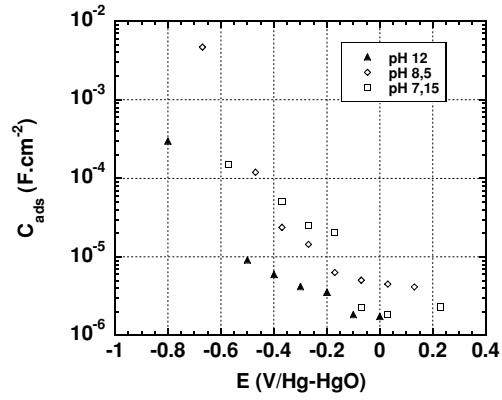

Figure 7 Changes in adsorption capacitance as a function of potential in the three solutions.

was negligible. Thus:

$$1/C_{\text{int}}^2 \approx 1/C_{\text{SC}}^2 = [(2)/(q\varepsilon\varepsilon_0 N)][E - E_{\text{bp}} - (K_{\text{B}}T/q)] \quad (6)$$

where E_{bp} is the flat band potential, ε the dielectric constant of the passive film ($\varepsilon = 12$) [10], ε_0 the permittivity of free space, N the majority carrier concentration, K_{B} the Boltzmann constant, and q the electron charge. E_{bp} and N were estimated from the Mott-Schottky diagrams (Fig. 6). The space charge layer thickness, when the space charge layer is approximated by a flat capacitor was determined according to the equation:

$$d = [(2\varepsilon\varepsilon_0)/(qN_{\text{D}})]^{1/2}[E - E_{\text{bp}} - (K_{\text{B}}T/q)]^{1/2} \quad (7)$$

The different experimental values obtained are shown in Table III. E_{corr} were always lower than the flat band potential ($E_{\text{cor}} \approx -170$ mV/Hg-HgO) indicating that the passive film (p-SC) was depleted at corrosion potential and that the space charge was negative. E_{bp} varied as a function of pH, although their variation was much greater than 60 mV per pH unit. This may be related to the equilibrium of boron-containing ions in this pH range [7]. The high dopant concentrations ($N \approx 10^{21}$ cm^{-3}) showed the high defectiveness, characteristic of a passive layer [11]. The low space charge layer thickness (calculated for $E - E_{\text{bp}} = 0.5$ V/Hg-HgO), was consistent with a highly doped passive layer.

The variation in adsorption capacitance (C_{ads}) as a function of potential in the three solutions was the same in all three solutions (Fig. 7). C_{ads} is maximum for a fractional coverage $\theta = 0.5$ and was observed for nickel oxidation potential (reaction 1). On the passivation plateau, C_{ads} values were of the same order of magnitude as those of the interfacial capacitances (50 μF/cm^2). It can thus be concluded that there was little adsorption in the investigated potential region.

TABLE III Semiconducting properties of the passive layer

	Solution 1 pH 12	Solution 2 pH 8.5	Solution 3 pH 7.15
E_{bp} (V/Hg-HgO)	0.236	0.624	0.896
N (cm^{-3})	7.2×10^{21}	4.3×10^{21}	6.8×10^{21}
d (nm)	0.3	0.4	0.3

3.3. Electrochemical quartz crystal microbalance

The nickel electrode quartz crystal frequency vibration was measured versus time at corrosion potential as a function of lithium hydroxide and orthoboric acid concentrations. Starting solution was 200 mL of LiOH at a concentration of 1.6×10^{-3} mol $\cdot$ L^{-1}, at 25°C. Following frequency stabilisation, 20 mL of 1.6×10^{-1}mol $\cdot$ L^{-1} LiOH was first added. Then, increasing amounts of orthoboric acid (H_3BO_3) were added. Limit mass variations after stabilisation in time (Δm_{lim}) were determined from Sauerbrey's relationship [2]. They are shown in Table IV.

The addition (1) of a very small concentration of lithium hydroxide caused a variation in mass. This variation could only be due to adsorption of the species present in the solution, in this case hydroxide ions. The addition of a small amount of orthoboric acid (additions 2 and 3) did not have any significant effect on the mass of the adsorbed film, the mass variation being limited to 0.1 μg $\cdot$ cm^{-2}. The adsorbed film was still essentially composed of the hydroxide species present in the solution. When larger amounts of orthoboric acid (additions 3–6) were added, the mass of this film increased regularly, going from 1.2 to 6.5 μg $\cdot$ cm^{-2} with pH variations from 11.5 to 7.5. This variation in mass can be attributed to different factors:

– adsorption of new species (borate ions) present in the solution at a higher concentration or at a more acid pH,

– modification of the passive layer at more acid pH values.

TABLE IV Variation in limiting mass (Δm lim) after stabilisation in time, as a function of LiOH and H_3BO_3 concentration on the nickel electrode

Additions	LiOH (mol $\cdot$ L^{-1})	H_3BO_3 (mol $\cdot$ L^{-1})	Δm lim (μg $\cdot$ cm^{-2})	pH
1	1.6×10^{-2}	—	1.1	11.6
2	1.6×10^{-2}	4.5×10^{-4}	1.2	11.5
3	1.6×10^{-2}	2.65×10^{-3}	1.25	11.1
4	1.6×10^{-2}	6.77×10^{-3}	1.65	9.4
5	1.6×10^{-2}	2.3×10^{-2}	3.85	8.4
6	1.6×10^{-2}	9.2×10^{-2}	6.5	7.5

Acidification of the medium leads to a reduction in hydroxide ion concentration. Desorption of the hydroxide ions with acidification of the solution should only lead to a reduction in the adsorbed mass. However this result was not obtained.

The nature of the adsorbed species originating from the boron differed according to pH. There was competition between the $H_2BO_3^-$, $B_4O_7^{2-}$ and $HB_4O_7^-$ ions. At pH = 11.2, the $H_2BO_3^-$ ions were in a majority, at pH = 9.37 it was the $B_4O_7^{2-}$ ions, while at pH 8.4 the adsorbed species were the $HB_4O_7^-$ ions [7]. For a given initial amount of boron in solution, the concentration of ions in solution ($H_2BO_3^-$, $B_4O_7^{2-}$, $HB_4O_7^-$) did not increase when the pH was decreased. The difference in borate ion distribution as a function of pH cannot provide justification for the increase in adsorbed mass.

Nickel corrosion occurring with an acidification of the solution could only lead to a loss of mass, which is not what was observed. The nickel thus remained passive in this pH range. This means that in the case of high orthoboric acid concentrations, the mass variation observed on the nickel electrode (Table IV) can be attributed only to the growth of passive layer in acidic solution.

The passive layer is modified as a function of pH. At high lithium hydroxide concentrations (high pH), the adsorbed film is not very hydrated [12]. The water molecules are generally found in the outer layers and are therefore very little adsorbed. The adsorbed film is therefore not as important. On the other hand, at low lithium hydroxide concentrations (less alkaline pH) the adsorbed film is more hydrated. The solute-solute forces have less influence on the cohesion of the film. The more hydrated adsorbed film is thus heavier.

In order to check our hypotheses, similar tests were carried out on the gold electrode. Since gold is a noble metal, it should have been possible to avoid formation of the passive layer. The factors concerned should be limited to adsorption phenomena. The gold electrode quartz crystal vibration frequency was measured in the same conditions as for the nickel electrode. The experimental results are given in Table V.

When large amounts of orthoboric acid were added (additions 3′–6′) no increases in adsorbed mass were observed despite the lower pH. This result confirms the role of the passive layer when large amounts of boric acid were added in the case of the nickel electrode. Only adsorption phenomena were measured on the gold electrode.

As in the previous case, the increase in mass with the first addition of lithium hydroxide (1′) was due to hydroxide ion adsorption. The addition of a small amount of orthoboric acid (additions 2′, 3′) had no significant effect on the mass of the adsorbed film. This film was still essentially composed of the hydroxide species present in solution. The mass of this adsorbed film increased up to pH 11.1 and was estimated at 13.4 $\mu g \cdot cm^{-2}$. From pH 9.4, the mass decreased, unlike the case of nickel. This variation can be attributed to the following:

– acidification of the medium, resulting in reduction of adsorbed hydroxide ions and therefore a reduction in the mass of the adsorbed film,

– change in the nature of the adsorbed species ($H_2BO_3^-$, $B_4O_7^{2-}$, $HB_4O_7^-$). The borate species concentration dropped when the pH of the solution was reduced on addition of boric acid (addition 3′).

The electrochemical quartz crystal microbalance measurements confirmed that there was no borate adsorption in the pH and potential conditions applied and that the passive layer formed was more hydrated when the pH became less alkaline. Furthermore, the results of the Auger spectrometry surface analyses showed that the passive layer formed in borate solution did not contain any borate and the thickness of this layer increased with the acidity of the solution.

TABLE V Variation in limiting mass (Δm lim) after stabilisation in time, as a function of LiOH and H_3BO_3 concentration on gold electrode

Additions	LiOH ($mol \cdot L^{-1}$)	H_3BO_3 ($mol \cdot L^{-1}$)	Δm lim ($\mu g \cdot cm^{-2}$)	pH
1′	1.45×10^{-2}	—	12.8	11.6
2′	1.45×10^{-2}	4.5×10^{-4}	13	11.5
3′	1.45×10^{-2}	2.65×10^{-3}	13.4	11.1
4′	1.45×10^{-2}	6.77×10^{-3}	11.3	9.4
5′	1.45×10^{-2}	2.3×10^{-2}	9.25	8.4
6′	1.45×10^{-2}	9.2×10^{-2}	9.75	7.5

4. Conclusion

The aim of this study was to investigate borate adsorption at the nickel and/or nickel oxide-electrolyte interface at various concentrations and pH in lithium and borate solutions. Cyclic voltammetry was used to define the nickel passivation range in a borate solution.

The electrochemical impedance diagrams obtained for nickel passivated in a borate solution presented a capacitive semi-circle at the highest frequencies and a more or less vertical straight line at the lowest frequencies. This was simulated by an equivalent electric circuit of an electrosorption reaction. The adsorption capacitance values were of the same order of magnitude as those of the interfacial capacitances. This means that in the pH and potential conditions applied there was very little adsorption. Impedance measurements were also used to determine the semiconducting properties of the nickel passive layer. Thus, the passive film that was formed was highly doped ($N \approx 10^{21}$ cm^{-3}) presented type p semi-conducting properties and was depleted in holes at the corrosion potential. In other words, the space charge layer was negative. Moreover, in the experimental conditions, the pH was higher than the iso-electric point of the nickel oxide ($pH_{pie} \approx 7.5$) [13]. The adsorption phenomena of a negative species were therefore not optimally promoted. For this to happen, a more acid solution (less than the pH of the iso-electric point) and a higher potential would be necessary.

The electrochemical quartz crystal microbalance measurements provided evidence that the hydroxide ions were adsorbed at the surface of the gold and nickel electrodes. On the other hand, the borate ions, by acidifying the solution, led to growth of the nickel passive layer, but they were not adsorbed on the surface of the film.

References

1. S. GARDEY, D. LINCOT and O. KERREC, Eurocorr'96, Nice, Septembre 1996.
2. G. SAUERBREY, *Zeitschrift für Physik* **155** (1999) 206.
3. J. LECOEUR, C. SELLA, J. C. MARTIN, L. TERTIAN and J. DESCHAMPS, *C.R. Acad. Sci. Paris série C* **l281** (1975) 71.
4. W. E. BERRY and R. B. DIEGLE, *EPRI Projects EPRI* **NP-552** (1979) 31.
5. N. SATO and K. KUDO, *Electrochim. Acta* **19** (1974) 461.
6. J. P. DIARD, B. LE GORREC and C. MONTELLA, "Cinétique Electrochimique" (Herman, Paris, 1996).
7. M. POURBAIX, "Atlas d'Equilibre Electrochimique à 25°C" (Gauthier-Villards, Paris, 1963).
8. M. BOJINOV, G. FABRICIUS, P. KINNUNEN, T. LAITINEN, K. MÄKELÄ, T. SAARO and G. SUNDHOLM, *J. Electroanal. Chem.* **504** (2001) 29.
9. B. R. MOISSAN, "Electrochemistry at Semiconductor and Oxidized Metal Electrodes" (Plenum Press-NY, 1980).
10. B. LOVRECEK and J. SEFAJA, *Electrochim. Acta* **17** (1972) 1151.
11. L. ANTONI, PhD Thesis, Institut National Polytechnique de Grenoble, France, 1996.
12. P. MARCUS, "Corrosion Localisée" (Edition de Physique, Les Ulis, 1994) p. 31.
13. B. S. MATHUR and B. VENKATARAMANI, *Coll. and Surf. A: Physicochem. and Engineer. Asp.* **140** (1998) 403.

Received 2 April 2002
and accepted 7 July 2003